



Cite this: DOI: 10.1039/d1tc01369f

Triazine-dibenzofuran-based n-type host materials for high-efficiency and long-lifetime green phosphorescent organic light-emitting diodes†

Dong Jun Kim,^{‡ab} Sunhee Lee,^{‡c} Yong Hui Lee,^b Hyungkeun Jang,^b
Kwang-Hyun Ahn^a and Won-Sik Han^{id}*^c

Effective host materials are required to improve the performance of phosphorescent organic light-emitting diodes (PhOLEDs). Herein, a series of triazine-dibenzofuran-based n-type host materials, **DBT1–DBT4**, was prepared by varying the substitution position of dibenzofuran. The photophysical, thermal, and electrochemical properties as well as the device performance of these materials were investigated to establish structure–property relationships. The results demonstrated that the substitution position of dibenzofuran significantly affects the chemical structure, resulting in differences in electrochemical and photophysical properties. All the developed materials were utilized in green top-emitting PhOLEDs as an n-type host material mixed with a p-type host (**BPCz**), and their electroluminescence (EL) properties were assessed by systematically analysing 18 devices. Among them, the green PhOLEDs using a mixed host of **DBT4/BPCz (DBP4-III)** displayed the best EL performance with a high current efficiency up to 131.98 cd A⁻¹, an external quantum efficiency up to 30.90%, and a power efficiency up to 105.44 lm W⁻¹ with a device lifetime (T_{95}) of 180 h at 10 000 nits. These findings are expected to aid in the development of improved n-type host materials for highly efficient top-emitting PhOLEDs with long operational lifetimes.

Received 25th March 2021,
Accepted 27th July 2021

DOI: 10.1039/d1tc01369f

rsc.li/materials-c

1. Introduction

Phosphorescent organic light-emitting diodes (PhOLEDs) have received considerable attention owing to their great potential in display and lighting applications because the heavy-metal phosphors used in these devices can theoretically achieve internal quantum efficiencies of 100% by harvesting both singlet and triplet excitons.^{1,2} However, heavy-metal phosphors cannot be directly used in PhOLED devices because they undergo self-quenching and triplet–triplet annihilation.^{3–6} To overcome this issue, heavy-metal phosphors are normally homogeneously dispersed in a host matrix. Therefore, the

development of high-performance host materials is essential for improving the performance of PhOLED devices. To realise an effective host–guest system for electroluminescent devices, the following requirements should be met: (i) the host material should possess good thermal stability and film-forming ability to extend the operational lifetime of the device;^{7,8} (ii) the triplet energy level (E_T) of the host material should be higher than that of the dopant material to allow complete energy transfer from the host to the heavy-metal phosphors and to confine the triplet excitons within the emitting layer;^{9–12} (iii) the lowest unoccupied molecular orbital (LUMO) level and the highest occupied molecular orbital (HOMO) level of the host should match those of the adjacent layers to facilitate charge injection at a lower driving voltage;^{13,14} and (iv) the host material should have bipolar charge transport properties to expand the charge recombination zone within the emissive layer, thus enhancing device efficiency.^{15,16} However, it is typically difficult to fully match the HOMO and LUMO energy levels of a single host with those of the adjacent layers to achieve balanced carrier injection, a low driving voltage, and high efficiency. In this regard, PhOLED devices with mixed-host systems have recently been fabricated to achieve a low driving voltage and high luminous efficiency.^{17–22} With two host materials, the mutual

^a Department of Applied Chemistry, Kyung Hee University, Yongin, Gyeonggi 17104, Republic of Korea

^b LT Materials Co., Yongin, Gyeonggi 17118, Republic of Korea

^c Department of Chemistry, Seoul Women's University, Seoul 01797, Republic of Korea. E-mail: wshan@swu.ac.kr

† Electronic supplementary information (ESI) available: Synthetic procedures and characterisation data, optimised structures, PL spectra in film state, PL spectra at 77 K, and cyclic voltammograms; physical properties of materials used for device construction, EOD data, and device data for control device and **DBT4-III** without CPL. See DOI: 10.1039/d1tc01369f

‡ These authors contributed equally to this work.

cooperation of hole- or electron-transport behaviour can markedly improve device performance. In particular, the combination of an n-type host with a p-type host imparts bipolar transport characteristics, thus broadening the exciton formation zone and balancing charge carrier injection and transport.²⁰

Dibenzofurans, which possess high triplet energies of up to 3.12 eV,²³ have been used as building blocks for the design of host materials.^{23–26} For example, Lee *et al.* reported a series of dibenzofuran-carbazole-based host materials, in which the photophysical and charge transport properties depended on the substitution position of dibenzofuran on the carbazole unit.²⁷ Notably, the selection of an appropriate substitution position was shown to be crucial for controlling the device performance of the host material. In addition, 1,3,5-triazine has been widely used in the design of donor–acceptor (D–A) luminescent systems because of its high π -deficiency.^{28–34} Moreover, owing to its ease of functionalisation, the charge-transfer and photophysical properties of 1,3,5-triazine can be tuned. However, the relationship between 1,3,5-triazine and dibenzofuran, including the effect of the substitution position of dibenzofuran, has not been comprehensively investigated.

In this study, we synthesized a series of potential n-type host materials based on dibenzofuran and biphenyl triazine, **DBT1–DBT4** (chemical structures are shown in Fig. 1). The effect of the substitution position of dibenzofuran on the thermal, photophysical, and electrochemical properties were investigated experimentally and using density functional theory (DFT) calculations to establish structure–property relationships. Finally, all the developed materials were utilised as n-type host materials mixed with a p-type host (9,9'-di(biphenyl-4-yl)-3,3'-bi(9*H*-carbazole; **BPCz**)) in green top-emitting PhOLEDs. Top-emitting device was chosen because this type of device has been considered to have advantages over the conventional bottom-emitting devices for integrating with active matrix displays and enhanced light-extraction efficiency.^{35–37} Therefore, research on top-emitting devices is still being actively continued to improve the device performances.^{38–43} Among the fabricated top-emitting PhOLEDs incorporating the four host materials developed in this work, the device using a mixed host of **DBT4/BPCz** displayed the best electroluminescence (EL) performances.

2. Experimental methods

2.1 General information

All experiments were performed in a dry nitrogen or argon atmosphere using standard Schlenk techniques. All solvents

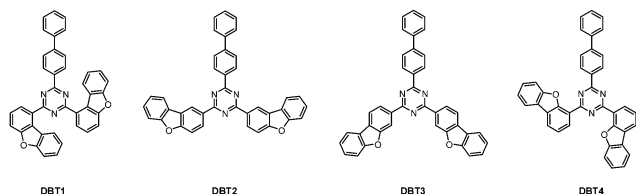


Fig. 1 Chemical structures of green host materials **DBT1–DBT4**.

were freshly distilled and used under dry nitrogen or argon purging. ¹H and ¹³C nuclear magnetic resonance (NMR) spectra were recorded using a Bruker Fourier 300 MHz spectrometer operated at 300.1 and 75.4 MHz, respectively. ¹H and ¹³C NMR spectra were measured in CDCl₃, and the ¹H and ¹³C chemical shifts were referenced to the residual solvent peaks at 7.26 and 77.16 ppm, respectively. Elemental analyses were performed using a Carlo Erba Instruments CHNS-O EA 1108 analyser. High-resolution mass spectrometry (HR-MS) analysis was performed using a highly sensitive liquid chromatography–multi-stage mass spectrometry (LC/MS/MS_n) (*n* = 10) system (Thermo Fisher Scientific, LCQ Fleet Hyperbolic Ion Trap MS/MS_n Spectrometer). Cyclic voltammetry (CV) was performed in an electrolytic solution consisting of 0.1 M *n*-Bu₄NPF₆ in dichloromethane at room temperature in an argon atmosphere using a potentiostat/galvanostat (Princeton Applied Research, PAR-STAT2273). ITO, Pt wire, and Ag/AgCl electrodes were used as the working, counter, and reference electrodes, respectively. All potentials were calibrated to the ferrocene/ferrocenium (Fc/Fc⁺) redox couple. Pd(PPh₃)₄, dibenzo[*b,d*]furan-1-ylboronic acid, dibenzo[*b,d*]furan-4-ylboronic acid, 3-bromodibenzofuran, 2-bromodibenzofuran, and 2-(4-biphenyl)-4,6-dichloro-1,3,5-triazine were purchased from Aldrich or TCI and used without further purification. The starting materials, *viz.* 2-(biphenyl-4-yl)-4,6-dichloro-1,3,5-triazine (**1**)⁴⁴ and *x*-dibenzofuranboronic acids (*x* = 1 (**2a**), 2 (**2b**), 3 (**2c**), and 4 (**2d**)),⁴⁵ were prepared by modifying previously reported methods.

2.2 Synthesis of **DBT1–DBT4**

The synthetic procedures and spectroscopic characterisation of **DBT1–DBT4** are described in the ESI.†

2.3 Absorption and emission spectra

The absorption and photoluminescence spectra were recorded on a Lambda 35 scanning spectrophotometer (PerkinElmer) and an LS55 fluorescence spectrophotometer (PerkinElmer), respectively. Phosphorescence emission spectra in 2-MeTHF at 77 K were collected using an F-7000 fluorescence spectrophotometer (Hitachi).

2.4 Thermal properties

Differential scanning calorimeter (DSC) and thermogravimetric analysis (TGA) were performed using a Mettler Toledo TGA/DSC1 instrument. Two TGA runs were conducted to confirm the results. The sample was loaded into a weight-tared alumina pan and heated at a rate of 10.00 °C min^{−1} from 10 to 600 °C under nitrogen flow (40–50 mL min^{−1}). The DSC experiments were carried in the temperature range of 30–400 °C in a nitrogen atmosphere. The sample was first heated at a rate of 10.00 °C min^{−1} and subsequently cooled at a rate of 10.00 °C min^{−1}.

2.5 DFT calculations

The DFT calculations were performed using the Gaussian16 package.⁴⁶ All structures were optimised using the DFT method with the B3LYP hybrid functional and a 6-31G(d,p) basis set. All calculations were performed in the gas phase.

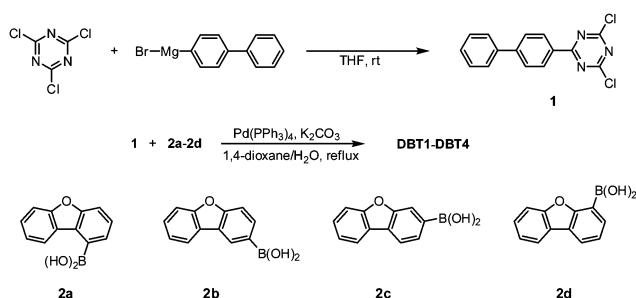
2.6 OLEDs device fabrications

For the OLED device fabrication, substrates of ITO(50 Å)/Ag(1000 Å)/ITO(50 Å) trilayer deposited glass (purchase from OTF Technology in Korea) were cut into 2.5×2.5 cm² squares and cleaned using detergent, acetone, and isopropanol in an ultrasonic bath. The organic layers used were deposited consecutively on ITO/Ag/ITO glass substrates by employing a thermal evaporation system at a pressure $< 1.0 \times 10^{-7}$ Torr. The samples were transferred to a vacuum thermal evaporator, and the organic layers and metal layer were subsequently deposited at a rate of 0.5 \AA s^{-1} (dopant: doping tooling factor $\times 10$) and 1 \AA s^{-1} , respectively. The detailed device structures are depicted in Fig. 5 with chemical structures of each material. The doping concentration of Ir(mdp)₃ in co-host is 6 wt%. To extract additional light from the devices and achieve both appropriate reflectivity and low absorption of the top contact for major emission wavelength of Ir(mdp)₃, a 63 nm-thick capping layer (CPL) was deposited on top of the Mg:Ag. The active device area of 4 mm² (2 mm \times 2 mm) was defined by the area of an overlap between the ITO and cathode (Mg:Ag) electrodes. Current, voltage, and luminance of the devices were measured with a system consisting of a Keithly, 2635A Source-Meter and a CS-2000 Spectro-radiometer. Operational lifetime measurements of the devices were taken in a constant current mode. LT95 values were determined from the decay traces of % luminance plotted as a function of operation time. Operation time at which the % luminance decreased to 95% corresponded to LT95. All the measurements were carried out at the room temperature under ambient atmosphere.

3. Results and discussion

3.1 Synthesis

Scheme 1 shows the synthetic procedures used to prepare DBT1–DBT4. Using a previously reported method with some modifications,⁴⁴ biphenyl-4-ylmagnesium bromide (Grignard reagent) was prepared by treating 4-bromobiphenyl with magnesium metal in tetrahydrofuran (THF). This Grignard reagent was reacted with cyanuric chloride to produce **1** in excellent yield ($> 80\%$). *x*-Dibenzofuranboronic acids ($x = 1$ (**2a**), 2 (**2b**), 3 (**2c**), and 4 (**2d**)) were prepared in modest yields according to a previously reported procedure⁴⁵ involving a direct substitution reaction between the corresponding bromodibenzofurans and



Scheme 1 Synthetic procedures for DBT1–DBT4.

trimethyl borate. Finally, DBT1–DBT4 were prepared *via* the Suzuki–Miyaura coupling reaction of **1** with dibenzofuranboronic acids **2a–2d** in the presence of Pd(PPh₃)₄ as a catalyst and excess amounts of base. The structures and chemical purities of the final products were verified by NMR spectroscopy, mass spectrometry, and elemental analysis (see ESI[†]).

3.2 Thermal properties

Host materials for efficient OLED devices require high thermally stable to prevent morphological changes and suppress aggregate formation upon heating. The thermal properties of DBT1–DBT4 were studied using DSC and TGA. As shown in Fig. 2a, none of the compounds exhibited a glass transition temperature (T_g) within the investigated temperature range (30–400 °C), even in the second and third DSC scans, which indicates that these materials will not undergo a phase change during device operation. The thermal decomposition temperatures (T_d , corresponding to 5% weight loss) of DBT1–DBT4 were 481, 466, 477, and 462 °C, respectively, as shown in Fig. 2b and Table 1. All the materials exhibited excellent thermal stability, making them suitable for PhOLED applications.

3.3 Theoretical calculations

To study the effect of the substitution position of dibenzofuran on the molecular geometry, geometrical optimisation of DBT1–DBT4 was performed using DFT calculations at the B3LYP/6-31G(d,p) level in the Gaussian16 package.⁴⁶ The

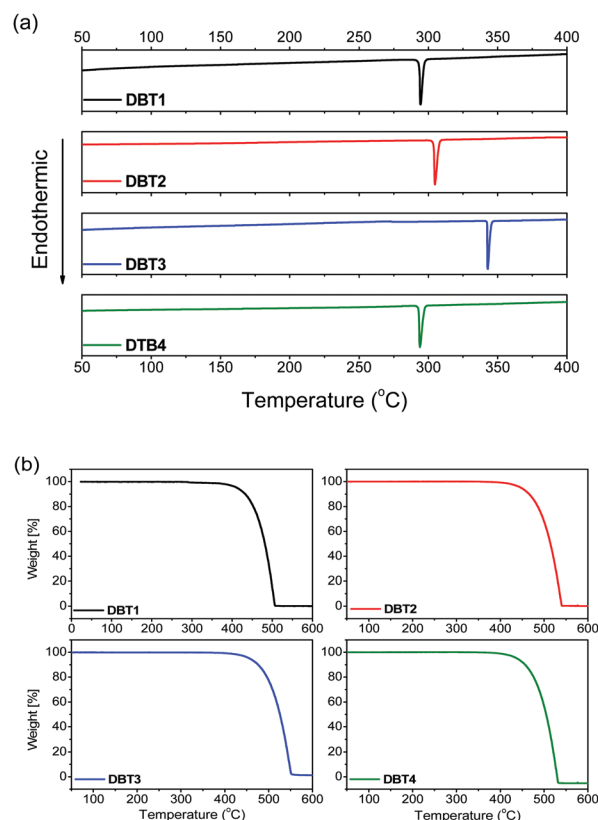


Fig. 2 (a) DSC and (b) TGA diagrams for DBT1–DBT4.

Table 1 Physical properties of **DBT1–DBT4**

	In THF solution		Film		E_T^b (eV)	T_d^c (°C)
	λ_{abs} (nm)	λ_{em} (nm)	λ_{em}^a (nm)			
DBT1	277, 324	404	414		2.56	481
DBT2	263, 300	377	399		2.57	466
DBT3	285, 326	380	420		2.63	477
DBT4	283, 315	425	433		2.56	462

^a Doped with **DBT1–DBT4** in PMMA film. ^b Measured in 2-MeTHF at 77 K. ^c Corresponding to a 5% weight loss.

optimised structures are depicted in Fig. S1 (ESI[†]). For **DBT2–DBT4**, the two dibenzofuran groups and the central triazine ring had planar geometries with dihedral angles (φ_1 and φ_2) close to 0°. In contrast, for **DBT1**, dihedral angles φ_1 and φ_2 were 22.9° and 28.2°, respectively, whereas the dihedral angle between the phenyl group and the central triazine ring (φ_3) was 8.8°. These results suggest that the molecular structure of **DBT1** is distorted due to steric hindrance. The energy levels and distribution of the HOMOs and LUMOs are shown in Fig. 3. For **DBT1–DBT3**, the HOMOs were mainly delocalised on the dibenzofuran unit with a small contribution from the central triazine. In contrast, for **DBT4**, the HOMO was distributed on both the dibenzofuran and biphenyl units. The distributions of the LUMOs also varied depending on the substitution position. The LUMOs of **DBT1–DBT3** were mainly delocalised over the biphenyl unit to the central triazine, whereas that of **DBT4** was mainly delocalised over the dibenzofuran unit to the central triazine, with a very small contribution from the biphenyl unit, which indicates intramolecular charge transfer (ICT) state would be significantly formed in the excited state.

3.4 Photophysical properties

To investigate the photophysical properties of **DBT1–DBT4**, the UV/Vis absorption and photoluminescence spectra in THF were recorded at room temperature. All compounds exhibited an absorption band at <280 nm (Fig. 4a), which is assigned to the π - π^* transitions of the biphenyl unit and the n - π^* transitions

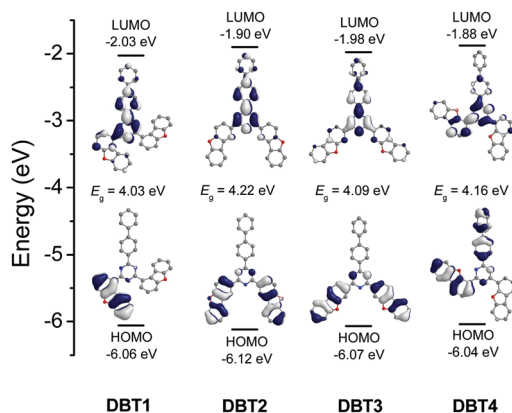


Fig. 3 Optimised structures of **DBT1–DBT4** and HOMO/LUMO distributions and energy levels obtained using the B3LYP/6-31G(d,p) method.

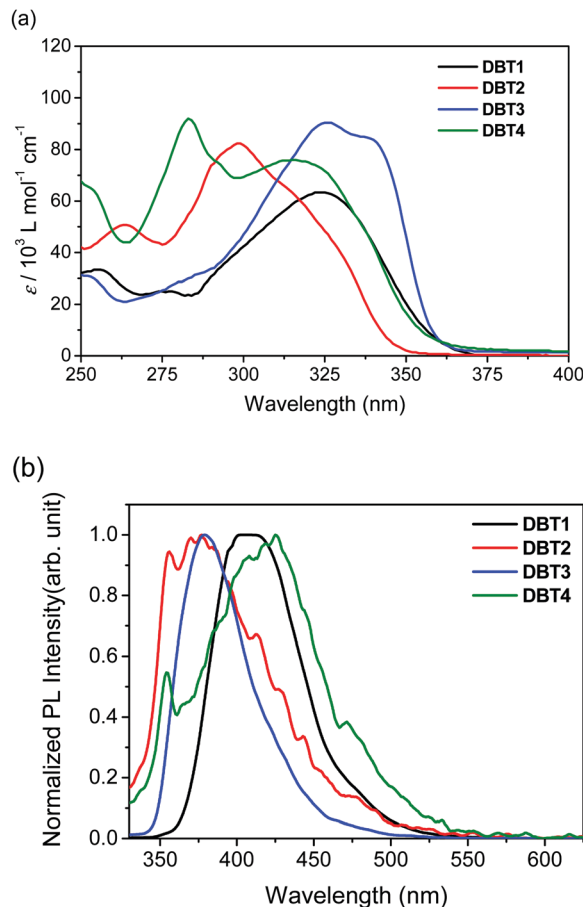


Fig. 4 (a) Absorption and (b) emission spectra of **DBT1–DBT4** in THF solution.

of the central triazine unit. In addition, additional broad absorption bands at ≥ 300 nm were observed (Fig. 4a and Table 1), which mainly originate from ICT transitions. For **DBT2**, the π - π^* transitions of the biphenyl group and the n - π^* transitions of the triazine rings might be predominant over ICT transitions, inducing hypsochromically shifted absorption bands. Accordingly, the optical bandgap of **DBT2** (3.53 eV), as calculated from the absorption edge of the UV/Vis spectra, was significantly larger than those of **DBT1** (3.34 eV), **DBT3** (3.39 eV), and **DBT4** (3.41 eV).

The emission spectra of **DBT1–DBT4** were measured by exciting 320 nm in THF solution (Fig. 4b) and film states (Fig. S2, ESI[†]). In the solution state, **DBT2** and **DBT3** showed their emission in a similar region at 380 nm, while **DBT1** and **DBT4** showed red-shifted emission bands at 404 nm and 425 nm, respectively. In the film state, all compounds showed bathochromic shift compared with their emission in the solution state. Among them, **DBT3** showed the largest bathochromic shift from 380 nm in solution to 420 nm in film. **DBT2** also showed a relatively large bathochromic shift from 380 nm to 400 nm. These relatively large bathochromic shifts in **DBT2** and **DBT3** would be due to their rotatable geometries in solution state attain geometrical planarity in film state, which increases their conjugation and results in a large bathochromic shift.

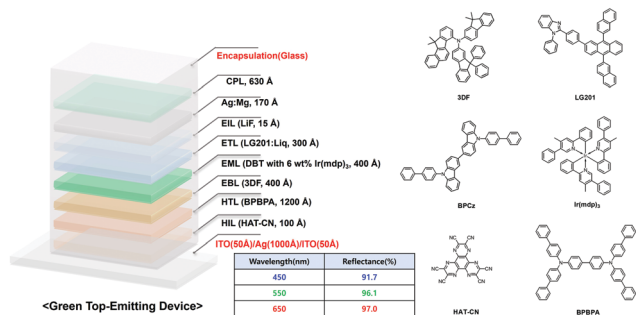


Fig. 5 Device structure and molecular structures of each material.

On the other hand, **DBT1** and **DBT4**, which have steric hindrances between dibenzofuran groups and the central triazine core, showed smaller bathochromic shifts from 403 and 425 nm to 414 and 433 nm, respectively.

The triplet energy level of a host material is important for use in PhOLEDs because back energy transfer from the triplet state of the dopant to the triplet state of the host decreases the emission efficiency.^{9–12} To investigate the triplet energy levels of **DBT1–DBT4**, the emission spectra were measured in 2-MeTHF at 77 K (Fig. S3, ESI†). All the compounds had similar triplet energy levels (2.55–2.57 eV), as estimated by taking the highest-energy phosphorescence peak as the T_1/S_0 transition energy, which corresponds to the vibronic 0–0 transition between these two electronic states. As the triplet energies of **DBT1–DBT4** are higher than that of **Ir(mdp)₃** ($E_T = 2.39$ eV),⁴⁷ they are sufficient to confine the triplet excitons on the green dopant and to prevent energy back transfer from the dopant to the host material.

3.5 Electrochemical properties

To investigate the electrochemical properties of **DBT1–DBT4**, cyclic voltammetry (CV) measurements were conducted in a 0.1 M tetra(*n*-butyl)ammonium hexafluorophosphate (*n*-Bu₄NPF₆) dichloromethane solution. The electrochemical properties are summarised in Table 2. As shown in Fig. S4 (ESI†), **DBT2–DBT4** exhibited oxidation peaks at 1.94, 1.97, and 1.98 V (vs. Fc/Fc⁺), respectively. In contrast, the oxidation peak of **DBT1** was observed at a more positive potential of 2.11 V. These peaks can be ascribed to the reduced forms of the benzofuran and biphenyl units. The reduction peak potentials for **DBT1**, **DBT2**, and **DBT4** were similar (−1.34, −1.32, and −1.33 eV, respectively), whereas the reduction peak of **DBT3** was observed

Table 2 Electrochemical properties of **DBT1–DBT4**

	E_{ox} (V)	E_{red} (V)	HOMO ^a (eV)	LUMO ^b (eV)	E_g (eV)	$E_g^{opt c}$ (eV)
DBT1	2.11	−1.34	−6.40	−2.95	3.45	3.34
DBT2	1.94	−1.32	−6.11	−2.86	3.56	3.53
DBT3	1.97	−1.69	−6.14	−2.47	3.47	3.39
DBT4	1.98	−1.33	−6.15	−2.83	3.50	3.41

^a HOMO (eV) = $-e(E_{ox}(\text{V vs. Fc/Fc}^+) + 4.8 \text{ eV})$. ^b LUMO (eV) = $-e(E_{red}(\text{V vs. Fc/Fc}^+) + 4.8 \text{ eV})$. ^c Calculated from the absorption edge of the UV/Vis spectra, $E_g^{opt} = 1240/\lambda_{onset}$.

at a more negative potential of −1.69 V. From the oxidation potentials, the energy levels of the HOMOs in **DBT1–DBT4** were estimated to be −6.40, −6.11, −6.14, and −6.15 eV, respectively, and the energy levels of the LUMOs were estimated to be −2.95, −2.86, −2.47, and −2.83 eV, respectively, from the reduction potentials.

3.6 Electron-only devices (EODs)

To compare the electron-transport properties of **DBT1–DBT4**, EODs containing each compound were fabricated. Fig. S5 (ESI†) showed the results of electrical measurements on single-carrier devices with the structures of ITO/Mg(150 Å)/Host(2000 Å)/Yb/Mg(200 Å). Using the space charge limited current (SCLC) model, which is characterized by field dependent mobility,^{48,49} the electron mobilities (μ_e) of **DBT1–DBT4** were estimated to be 1.30×10^{-7} , 8.49×10^{-9} , 8.50×10^{-8} , and 1.30×10^{-9} cm² V^{−1} s^{−1}, respectively.

3.7 Device performances

To evaluate the suitability of **DBT1–DBT4** as n-type hosts in PhOLEDs, five types of top-emitting OLED devices were fabricated for each n-type host. First, a device using only p-type host in the emissive layer was fabricated as a **control device**. Device **type I** was fabricated using only n-type hosts without a p-type host. Device **types II, III, and IV** were fabricated with mixed host systems with the n-type host and mixed with **BPCz** as a p-type host at ratios of 1:1, 1:2, and 2:1, respectively. The device configuration was as follows: HAT-CN (100 Å)/BPBPA (1200 Å)/3DF (400 Å)/emissive layer (EML; host(s) doped with 6 wt% **Ir(mdp)₃** (400 Å))/LG201:Liq = 2:1 (300 Å)/LiF (15 Å)/Mg:Ag = 1:10 (170 Å)/CPL (630 Å), in which **HAT-CN** was used as a hole-injecting material (HIM), **BPBPA** as a hole-transporting material (HTM), **3DF** as an electron-blocking material (EBM), **Ir(mdp)₃** as an emissive dopant, **LG201:Liq** as an electron-transporting material (ETM), and LiF as an electron-injecting material (EIM). The molecular structures and energy level diagrams of these materials are shown in Fig. 5, and their physical properties are summarised in Table S1 (ESI†).

In control device, without n-type host, the turn-on voltage was 2.80 V and the device efficiencies were very low with a current efficiency of 13.73 cd A^{−1}, an EQE of 3.18%, and a power efficiency of 4.43 lm W^{−1}, as shown in Fig. S6 (ESI†) and Table 3.

When using only n-type host materials, **DBT1–DBT4**, the **type I** devices (**DBT1-I–DBT4-I**) exhibited relatively low turn-on voltages (<2.5 V; brightness of 1 nit), as shown in Fig. 6. However, all the **type I** devices exhibited still very low device efficiencies with external quantum efficiency (EQE) values of 4.80–12.80%. Among them, **DBT2-I** exhibited a bathochromically shifted EL spectra. Moreover, the emission profiles differed from that of the dopant at approximately 430 nm (inset, Fig. 6c (logarithmic scale)), which indicates that the **type I** devices might contain excess electrons in the EML, resulting in the generation of an emission zone on the surface of the HBL (3DF) layer. It should be noted that the device lifetimes were also very short (T_{95} at 15 000 nits >3 h). Device **types II, III, and**

Table 3 Electroluminescence characteristics of fabricated green PhOLEDs

Devices	@10 000 nits						@15 000 nits			
	Turn-on voltage (V)	EL efficiency (cd A ⁻¹)	Power efficiency (lm W ⁻¹)	EQE (%)	λ_{\max} (nm)	FWHM (nm)	CIE		T_{95} (h)	
							x	y		
Control device (n/p = 0:1)	2.80	13.73	4.43	3.18 (3.18) ^a	531	39	0.280	0.692	—	
Type I (n/p = 1:0)	DBT1-I	2.01	28.81	18.90	6.66 (14.99) ^a	431, 536	38	0.272	0.695	2
	DBT2-I	2.21	21.02	11.30	4.80 (15.27) ^a	429, 550	46	0.321	0.656	1
	DBT3-I	2.09	31.47	18.43	7.24 (17.34) ^a	431, 538	37	0.275	0.694	1
	DBT4-I	2.49	54.82	32.84	12.80 (30.57) ^a	430, 534	35	0.253	0.710	3
Type II (n/p = 1:1)	DBT1-II	2.04	72.23	48.29	17.88 (28.81) ^a	525	28	0.205	0.739	100
	DBT2-II	2.19	89.82	71.64	20.79 (36.32) ^a	536	37	0.264	0.705	38
	DBT3-II	2.09	91.92	61.24	21.32 (31.04) ^a	535	34	0.259	0.709	140
	DBT4-II	2.06	117.46	94.16	27.58 (38.06) ^a	531	32	0.244	0.719	75
Type III (n/p = 1:2)	DBT1-III	2.06	101.09	69.48	23.22 (33.14) ^a	527	29	0.205	0.739	250
	DBT2-III	2.21	121.99	95.54	28.22 (35.71) ^a	536	37	0.266	0.703	33
	DBT3-III	2.06	115.29	81.34	26.76 (32.33) ^a	534	34	0.259	0.710	275
	DBT4-III	2.20	131.98	105.44	30.90 (36.98) ^a	533	33	0.250	0.715	180
	DBT4-III without CPL	2.20	94.07	67.36	21.28 (26.0) ^a	555	43	0.328	0.653	—
Type IV (n/p = 2:1)	DBT1-IV	2.04	50.05	31.43	12.32 (24.10) ^a	526	28	0.207	0.738	35
	DBT2-IV	2.12	58.36	43.54	13.44 (33.79) ^a	538	38	0.269	0.701	26
	DBT3-IV	2.12	63.34	38.93	14.68 (28.45) ^a	535	34	0.258	0.710	30
	DBT4-IV	2.06	105.29	80.08	24.86 (37.16) ^a	531	32	0.239	0.722	26

^a Values in parentheses indicate maximum EQE values.

IV with mixed hosts were fabricated to balance the holes/electrons and optimise the device structure. The overall EL performance of these devices is shown in Fig. 7–9 and Table 3. In device **types II–IV**, the additional emission at approximately 430 nm disappeared, indicating complete and effective energy transfer from the host to the dopant during the EL process and that the EL emission originates from the triplet excited state of the phosphor. Accordingly, the efficiencies of device **types II–IV** with mixed host systems were at least two times higher those of device **type I** with a single host. All **type II** devices, which had a n-type/p-type host ratio of 1:1, showed superior efficiency at 10 000 nits as compared to the corresponding **type I** devices (Table 3). This significant improvement in device performance might originate from a broadened recombination zone and balanced charge carrier injection and transport owing to the n-type/p-type mixed host system in the EML. As shown in Fig. 7, **DBT4-II**, showed the best device performance among the **type II**

devices with a current efficiency of 117.46 cd A⁻¹, an EQE of 27.58%, and a power efficiency of 94.16 lm W⁻¹. In contrast, device **DBT1-II** showed the lowest device performance with a current efficiency of 72.23 cd A⁻¹, an EQE of 17.88%, and a power efficiency of 48.29 lm W⁻¹. Nevertheless, the device performance of **DBT1-II** was significantly improved compared to that of **DBT1-I**. The high efficiency of **DBT4-II** clearly indicates that **DBT4** is the most suitable host among **DBT1–DBT4** because all the devices were identical except for the n-type host material. The superior performance of **DBT4-II** should benefit from improved electron and hole injection and transportation, originating from the better charge balancing abilities of **DBT4**. Although **DBT1** also exhibited bipolar characteristics, **DBT1-II** showed a lower device efficiency owing to the deeper HOMO and LUMO energy levels, that is, the electron concentration in the EML increased, making the carriers less balanced.

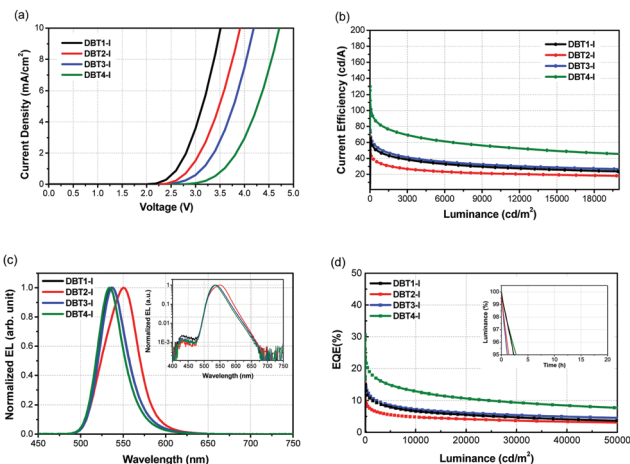


Fig. 6 Performance of **type I** devices. (a) Current density–voltage, (b) current efficiency–luminance, (c) EL spectra, and (d) EQE–luminance (inset: operational lifetime (T_{95} @ 15 000 nits)).

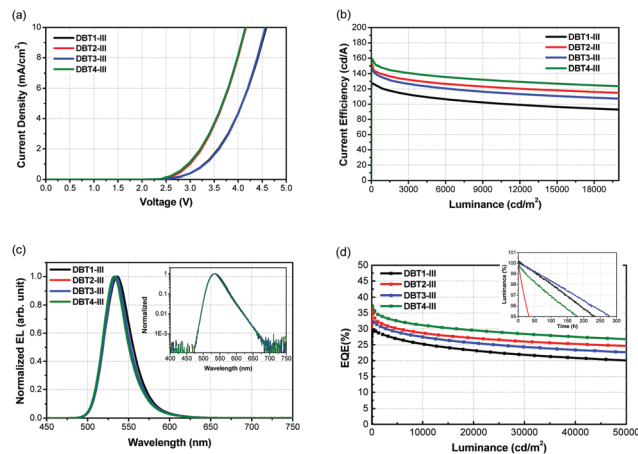


Fig. 8 Performance of **type III** devices. (a) Current density–voltage, (b) current efficiency–luminance, (c) EL spectra, and (d) EQE–luminance (inset: operational lifetime (T_{95} @ 15 000 nits)).

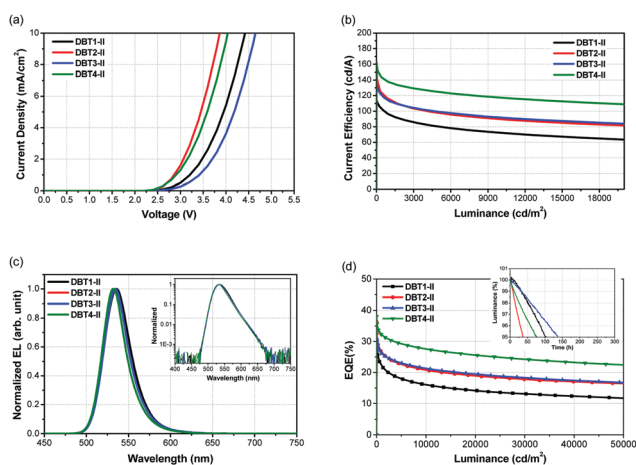


Fig. 7 Performance of **type II** devices. (a) Current density–voltage, (b) current efficiency–luminance, (c) EL spectra, and (d) EQE–luminance (inset: operational lifetime (T_{95} @ 15 000 nits)).

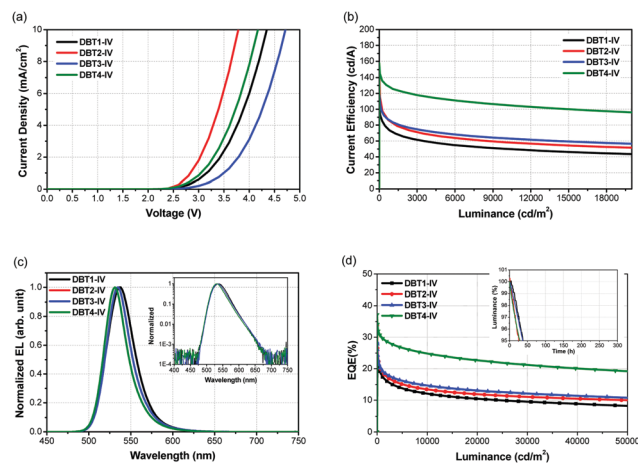


Fig. 9 Performance of **type IV** devices. (a) Current density–voltage, (b) current efficiency–luminance, (c) EL spectra, and (d) EQE–luminance (inset: operational lifetime (T_{95} @ 15 000 nits)).

When the ratio of the p-type host was increased (**device type III**), all the devices exhibited higher device efficiency as compared to the corresponding **type II** devices (Fig. 8). Similar trends were observed for device **types II** and **III**, with the device efficiencies gradually increasing in the order **DBT1**, **DBT3**, **DBT2**, and **DBT4**. For **DBT4-III**, the turn-on voltage was 2.2 V with a current efficiency of 131.98 cd A^{-1} , an EQE of 30.90%, and a power efficiency of 105.44 lm W^{-1} at 10 000 nits. Because **DBT1** had mismatched HOMO and LUMO energy levels, **DBT1-III** exhibited the lowest efficiency with a current efficiency of 101.09 cd A^{-1} , an EQE of 24.64%, and a power efficiency of 69.48 lm W^{-1} .

As shown in Fig. 9, when the ratio of n-type host was increased (**device type IV**), all the devices exhibited decreased device efficiency as compared to the corresponding **type II** devices. This result can be rationalised by an unbalanced carrier density in device **type IV** owing to the hole transport properties being poorer than the electron transport properties.

The same device efficiency trend was observed for device **type IV** as for device **types II** and **III**. It should be noted that the maximum EQE of **DBT4-III** was 36.98% at $10\,000 \text{ cd m}^{-2}$, as shown in Fig. 8(d).

To further study the CPL effect in the device performance, we fabricated additional device which has a same structure with **DBT4-III** but without CPL. As shown in Fig. S7 (ESI[†]) and Table 3, the device without CPL showed but enlarged FWHM from 32 nm to 43 nm and the EQE was dropped from 30 to 21% to compared with **DBT4-III**. Also, the EL spectrum was red-shifted compared with **DBT4-III**. These results indicate that the CPL has a role as an optical functional to enhance the emissions and adjust the spectral distributions.^{50–52}

Because lifetime performance is one of the most important factors in PhOLEDs, the device operational lifetime (T_{95}) of each device was measured under constant conditions (15 000 nits). In general, the **type III** devices exhibited the longest operational

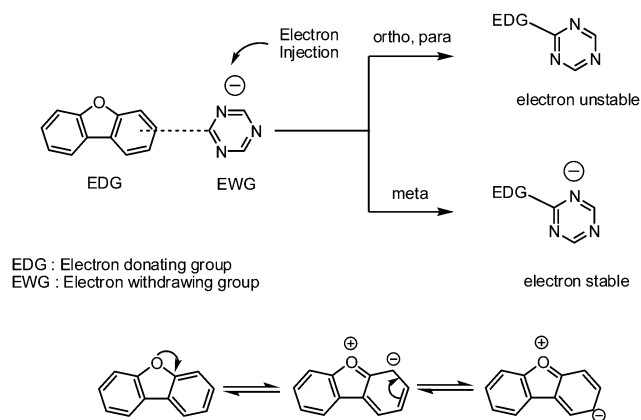


Fig. 10 Directing effects in **DBT1–DBT4**.

lifetimes, with **DBT3-III** showing the longest device lifetime of 275 h, followed by **DBT1-III** (200 h), **DBT4-III** (180 h), and **DBT2-III** (33 h). It should be noted that the mixed-host PhOLEDs (device types **II** and **III**) exhibited significantly improved luminance decay characteristics as compared to the single-host PhOLEDs (device type **I**). Moreover, it was found that the substitution position significantly affected the device lifetime. Namely, substitution of the triazine groups at the 1 and 3 positions of dibenzofuran (**DBT1** and **DBT3**) resulted in relatively longer lifetimes than substitution at the 2 and 4 positions (**DBT2** and **DBT4**). This would be rationalised by directing effects of substituents in conjugation with the aromatic ring, as shown in Fig. 10. In the case of **DBT1** and **DBT3**, the triazine unit is substituted at the *meta*-position from the oxygen atom of dibenzofuran, which would not affect the stabilisation of the injected electrons. On the other hand, injected electrons in **DBT2** and **DBT4** would be stabilised since the triazine unit is positioned at the *ortho*- and *para*-positions, respectively.

4. Conclusions

In this study, the effect of the substitution position of dibenzofuran on the photophysical properties and device performance of a series of triazine-dibenzofuran derivatives (**DBT1–DBT4**) were systematically investigated. The substitution position had a significant effect on the efficiency curves of the devices incorporating **DBT1–DBT4** as n-type host materials. In addition, when p-type host material **BPCz** was mixed with these n-type hosts in the EML, the device efficiencies were significantly improved. In particular, **DBT4** showed excellent device performances owing to its appropriate energy levels. The mixed-host device using this material at an n-type/p-type host ratio of 1 : 2 (**DBT4-III**) had a low turn-on voltage of 2.2 V with an EQE of 30.90% and a high-power efficiency of 105.44 lm W⁻¹, which is one of the highest power efficiencies reported for green top-emitting PhOLEDs. Moreover, **DBT4-III** exhibited an excellent operational lifetime (T_{95}) of 180 h at an initial luminance of 15 000 nits. The systematic study of structure–property relationships for host materials provides important

strategies for developing efficient n-type hosts to achieve high-efficiency and long-lifetime PhOLEDs.

Conflicts of interest

There are no conflicts to declare.

Acknowledgements

This work was supported by the National Research Foundation of Korea (2019R1F1A1058578) and the Technology Innovation Program (20010484) funded by the Ministry of Trade, Industry & Energy (MOTIE, Korea).

References

- M. A. Baldo, D. F. O'Brien, Y. You, A. Shoustikov, S. Sibley, M. E. Thompson and S. R. Forrest, *Nature*, 1998, **395**, 151–154.
- M. A. Baldo, M. E. Thompson and S. R. Forrest, *Nature*, 2000, **403**, 750–753.
- C. Adachi, R. Kwong and S. R. Forrest, *Org. Electron.*, 2001, **2**, 37–43.
- C. Adachi, M. A. Baldo, S. R. Forrest and M. E. Thompson, *Appl. Phys. Lett.*, 2000, **77**, 904–906.
- Q. S. Zhang, Q. G. Zhou, Y. X. Cheng, L. X. Wang, D. G. Ma, X. B. Jing and F. S. Wang, *Adv. Mater.*, 2004, **16**, 432–436.
- S.-J. Yeh, M.-F. Wu, C.-T. Chen, Y.-H. Song, Y. Chi, M.-H. Ho, S.-F. Hsu and C.-H. Chen, *Adv. Mater.*, 2005, **17**, 285–289.
- Y. Tao, C. Yang and J. Qin, *Chem. Soc. Rev.*, 2011, **40**, 2943–2970.
- Z. Ge, T. Hayakawa, S. Ando, M. Ueda, T. Akiike, H. Miyamoto, T. Kajita and M. Kakimoto, *Adv. Funct. Mater.*, 2008, **18**, 584–590.
- S. Tokito, T. Iijima, Y. Suzuri, H. Kita, T. Tsuzuki and F. Sato, *Appl. Phys. Lett.*, 2003, **83**, 569–571.
- W.-S. Han, H.-J. Son, K.-R. Wee, K.-T. Min, S. Kwon, I.-H. Suh, S.-H. Choi, D. H. Jung and S. O. Kang, *J. Phys. Chem. C*, 2009, **113**, 19686–19693.
- Y. Tao, Q. Wang, C. Yang, C. Zhong, K. Zhang, J. Qin and D. Ma, *Adv. Funct. Mater.*, 2010, **20**, 304–311.
- M. Romain, S. Thiery, A. Shirinskaya, C. Declairieux, D. Tondelier, B. Geffroy, O. Jeannin, J. Rault-Berthelot, R. Metivier and C. Cyril Poriel, *Angew. Chem., Int. Ed.*, 2015, **54**, 1176–1180.
- D. F. O'Brien, M. A. Baldo, M. E. Thompson and S. R. Forrest, *Appl. Phys. Lett.*, 1999, **74**, 442–444.
- R. J. Holmes, B. W. D'Andrade, S. R. Forrest, X. Ren and M. E. Thompson, *Appl. Phys. Lett.*, 2003, **83**, 3818–3820.
- E. L. Williams, K. Haavisto, J. Li and G. E. Jabbour, *Adv. Mater.*, 2007, **19**, 197–202.
- C. Murawski, K. Leo and M. C. Gather, *Adv. Mater.*, 2013, **25**, 6801–6827.

- 17 M. E. Kondakova, T. D. Pawlik, R. H. Young, D. J. Giesen, D. Y. Kondakov, C. T. Brown, J. C. Deaton, J. R. Lenhard and K. P. Klubek, *J. Appl. Phys.*, 2008, **104**, 094501.
- 18 J. Lee, J.-I. Lee, J. Y. Lee and H. Y. Chu, *Appl. Phys. Lett.*, 2009, **95**, 253304.
- 19 N. Chopra, J. S. Swensen, E. Polikarpov, L. Cosimbescu, F. So and A. B. Padmaperuma, *Appl. Phys. Lett.*, 2010, **97**, 033304.
- 20 Y. C. Chen, J. Chen, Y. Zhao and D. Ma, *Appl. Phys. Lett.*, 2012, **100**, 213301.
- 21 D. Liu, F. Wang and R. Yao, *J. Mater. Chem. C*, 2018, **6**, 7839–7846.
- 22 D. S. Kim, K. H. Lee and J. Y. Lee, *ACS Appl. Mater. Interfaces*, 2020, **12**, 19737–19745.
- 23 P. A. Vecchi, A. B. Padmaperuma, H. Qiao, L. S. Sapochak and P. E. A. Burrows, *Org. Lett.*, 2006, **8**, 4211–4214.
- 24 S. H. Jeong and J. Y. Lee, *Org. Electron.*, 2012, **13**, 1141–1145.
- 25 Y. Im and J. Y. Lee, *Dyes Pigm.*, 2015, **113**, 743–747.
- 26 C. Han, G. Xie, J. Li, Z. Zhang, H. Xu, Z. Deng, Y. Zhao, P. Yan and S. Liu, *Chem. – Eur. J.*, 2011, **17**, 8947–8956.
- 27 C. W. Lee, J.-A. Seo, M.-S. Gong and J. Y. Lee, *Chem. – Eur. J.*, 2013, **19**, 1194–1198.
- 28 F. Pop, F. Riobé, S. Seifert, T. Cauchy, J. Ding, N. Dupont, A. Hauser, M. Koch and N. Avarvari, *Inorg. Chem.*, 2013, **52**, 5023–5034.
- 29 Y.-J. Cho, A.-R. Lee, S.-Y. Kim, M. Cho, W.-S. Han, H.-J. Son, D. W. Cho and S. O. Kang, *Phys. Chem. Chem. Phys.*, 2016, **18**, 22921–22928.
- 30 S. Y. Lee, T. Yasuda, H. Nomura and C. Adachi, *Appl. Phys. Lett.*, 2012, **101**, 093306.
- 31 W. Zhang, C. Zhu, Z. Huang, C. Gong, Q. Tang and X. Fu, *Org. Electron.*, 2019, **67**, 302–310.
- 32 L. Su, F. Cao, C. Cheng, T. Tsuboi, Y. Zhu, C. Deng, X. Zheng, D. Wang, Z. Liu and Q. Zhang, *ACS Appl. Mater. Interfaces*, 2020, **12**, 31706–31715.
- 33 A. Puthanveedu, K. Shanmugasundaram, J. C. John and Y. Choe, *J. Phys. Chem. C*, 2020, **124**, 19273–19281.
- 34 S. Y. Lee, T. Yasuda, H. Nomura and C. Adachi, *Appl. Phys. Lett.*, 2012, **101**, 093306.
- 35 M.-H. Lu, M. S. Weaver, T. X. Zhou, M. Rothman, R. C. Kwong, M. Hack and J. J. Brown, *Appl. Phys. Lett.*, 2002, **81**, 3921–3923.
- 36 H. Riel, S. Karg, T. Beierlein, B. Ruhstaller and W. Rieß, *Appl. Phys. Lett.*, 2003, **82**, 466–468.
- 37 S. Chen, L. Deng, J. Xie, L. Peng, L. Xie, Q. Fan and W. Huang, *Adv. Mater.*, 2010, **22**, 5227–5239.
- 38 S. O. Jeon, K. H. Lee, J. S. Kim, S.-G. Ihn, Y. S. Chung, J. W. Kim, H. Lee, S. Kim, H. Choi and J. Y. Lee, *Nat. Photonics*, 2021, **15**, 208–215.
- 39 C. Zang, S. Liu, M. Xu, R. Wang, C. Cao, Z. Zhu, J. Zhang, H. Wang, L. Zhang, W. Xie and C.-S. Lee, *Light Sci. Appl.*, 2021, **10**, 116.
- 40 Y. Deng, C. Keum, S. Hillebrandt, C. Murawski and M. C. Gather, *Adv. Opt. Mater.*, 2021, **9**, 2001642.
- 41 Z. Bin, D. Shi, R. Su, W. Han, D. Zhang and L. Duan, *Sci. Bull.*, 2020, **65**, 153–160.
- 42 M. Jung, K. H. Lee, J. Y. Lee and T. Kim, *Mater. Horiz.*, 2020, **7**, 559–565.
- 43 S. K. Kim, R. Lampande and J. H. Kwon, *ACS Photonics*, 2019, **6**(11), 2957–2965.
- 44 S. K. Behzad, M. M. Amini, M. Ghanbari, M. Janghouri, P. Anzenbacher Jr. and S. W. Ng, *Eur. J. Inorg. Chem.*, 2017, 3644–3654.
- 45 S. Chen, Y. Wu, Y. Zhao and D. Fang, *RSC Adv.*, 2015, **5**, 72009–72018.
- 46 M. J. Frisch, *et al.*, *Gaussian 16, Revision C.01*, Gaussian, Inc., Wallingford CT, 2016.
- 47 X. Ma, J. Liang, F. Bai, K. Ye, J. Xu, D. Zhu and M. R. Bryce, *Eur. J. Inorg. Chem.*, 2018, 4614–4621.
- 48 P. N. Murgatroyd, *J. Phys. D: Appl. Phys.*, 1970, **3**, 151–156.
- 49 T. Y. Asuda, Y. Yamaguchi, D. C. Zou and T. Tsutsui, *Jpn. J. Appl. Phys.*, 2002, **41**, 5626–5629.
- 50 J. W. Huh, J. Moon, J. W. Lee, D.-H. Cho, J.-W. Shin, J.-H. Han, J. Hwang, C. W. Joo, J.-I. Lee and H. Y. Chu, *IEEE Photonics J.*, 2012, **4**, 39–47.
- 51 H. Riel, S. Karg, T. Beierlein and W. Rieß, *J. Appl. Phys.*, 2003, **94**, 5290–5296.
- 52 Q. Huang, K. Walzer, M. Pfeiffer and K. Leo, *J. Appl. Phys.*, 2003, **100**, 064507.